Influence of various metakaolin raw materials on the water and fire resistance of geopolymers prepared in phosphoric acid

Hélène Celerier, Jenny Jouin, Nicolas Tessier-Doyen, Sylvie Rossignol

Influence of various metakaolin raw materials on the water and fire resistance of geopolymers prepared in phosphoric acid

Hélène Celerier, Jenny Jouin, Nicolas Tessier-Doyen, Sylvie Rossignol*

IRCER, 12 rue Atlantis, 87068 Limoges Cedex, France

Different formulations of geopolymers were synthesized in acidic media (phosphoric acid) starting from three different raw metakaolin materials to identify compositions of interest. Four different property groups were highlighted based on the most favorable thermal and water resistance properties (while maintaining acceptable mechanical properties). The groups were related to the chemical composition, setting time and setting temperature of the synthesized geopolymers. Indeed, mechanical strength was determined by chemical composition, such as the aluminum content and the amount of water in each sample. The results showed that the sample with Si/Al ≥ 1 and Al/P = 1 exhibited compressive stress to rupture values ranging between 66 and 120 MPa and was thermal resistant. Water resistance with a mechanical strength of 50 MPa was obtained for the samples with Al/P = 1 or 4 and Si/Al ≤ 1. This work highlights the possibility of selecting a specific property associated with the mechanical performance for an acidic geopolymer.

1. Introduction

During the last several decades, a new class of materials called "geopolymers" belonging to the family of cements and concrete products has emerged. It was first reported in 1978 by Professor J. Davidovits [1], who has been recognized as a pioneer of such aluminosilicate-based materials. Geopolymers are very attractive materials because they can be used to manufacture precast structures, concrete pavement, and concrete products and to immobilize toxic waste that is resistant to heat and aggressive environments [2]. The synthesis of these geopolymers is based on the alkaline activation of aluminosilicates, which induces the formation of free $Si[OH]_4$ and $Al[OH]_4^-$ oligomers [3,4].

Many authors have investigated the parameters related to the formation, structure and physical properties of geopolymers [3,5,6]. Key factors for controlling the geopolymerization reaction in basic media, such as the roles of the aluminosilicate source and the alkaline solution, have been recently identified. This control requires perfect knowledge of the raw material characteristics and structure, including the reactivity. For example, for a metakaolin source, accurate quantification of surface reactivity is of interest: a high reactivity requires (i) a low molar ratio of Si/Al, (ii) a high wettability value, (iii) a large amount of amorphous phase, and finally, (iv) a great proportion of reactive tetrahedral aluminum (≤ 1.2, ≥ 760 µL/g, ≥ 63 wt%, and ≥ 19%, respectively) [7]. These data have been plotted to determine the location of geopolymers in the ternary diagram of Si-Al-M/O [8]. The relationship between the feasibility of the geopolymer preparation and the reactivity of the introduced raw materials has been highlighted. The existing domain of geopolymers is even more reduced when the reactivity of the raw materials is weak. Moreover, the concentrations of alkali and aluminum cations strongly affect the feasibility of these materials [9].

Another possible processing method consists in favoring the reaction of metakaolin in an acidic medium to produce an acidic geopolymer. In the preparation of an acidic geopolymer, the geopolymerization process begins with the dissolution of the aluminosilicate source, leading to the release of Al^{3+}. These aluminum ions react with phosphoric acid, leading to the formation of $AlPO_4$. The presence of $AlPO_4$ within the geopolymer has been observed by several authors [10,11], supporting this proposed mechanism of geopolymer formation. The aluminosilicate source whose aluminum has been dissolved also reacts with phosphoric acid, leading to the formation of a three-dimensional network of [Si-O-P]. Thus, the formed geopolymer consists of a three-dimensional network of [Si-O-P] and $AlPO_4$. The amount of acid affects the geopolymerization process as well as the structure and final properties of the geopolymer. Thus, if the Si/P ratio is decreased (i.e., the amount of acid is increased), a more amorphous geopolymer structure is formed due to improved dissolution [12]. The reactivity of

* Corresponding author.
E-mail address: sylvie.rossignol@unilim.fr (S. Rossignol).

the aluminosilicate source [11] also affects the geopolymerization process. The synthesis of acid-based geopolymers produces geopolymers with enhanced mechanical performances, as demonstrated by D.S. Perrera [13], where the geopolymers prepared in an acidic medium exhibited a two-fold higher resistance to compression (146 MPa) than the geopolymers synthesized in a basic medium (72 MPa). According to Perrera, this improvement in the properties can be related to a decrease in the pore volume fraction and/or to the presence of stronger bonds in the acidic geopolymer. Similarly, H.K. Tchakouté [10] observed an improvement in the mechanical properties of an acid-reacted geopolymer, typically exhibiting a compressive stress to rupture value near 93 MPa.

Materials exhibiting flame-retardant characteristics can be combined with other materials, such as polymers, to form a composite with improved fire-resistant properties [14]. According to Chiou [15], in the case of aluminum matrix composites, the presence of aluminum metaphosphate ($Al(PO_3)_3$) favors a high thermal resistance of up to at least 1000 °C. Moreover, Jiang [16] showed that the presence of silicon is beneficial for improving these properties, where a layer of silica that forms on the surface after heat treatment protects the material. In that study, silicon also reacted with phosphorous to form silicon pyrophosphate (SiP_2O_7, $Si_3(PO_4)_4$ and $Si_3P_6O_{25}$), which is known to improve the flame retardancy. Moreover, the use of a polymer matrix leads to the generation of smoke during heat treatment. Yan [17] demonstrated that the addition of nanosilica reduced the amount of smoke generated and enhanced the flame resistance. Thermal resistance is also observed in alkali-activated materials and was improved by the addition of fillers [18,19,20], such as refractory aluminosilicate particles and fibers. According to Bernal et al. [21], additives such as calcium powder can also improve the densification of materials during heat treatment.

The resistance of materials containing aluminum, silicon and phosphorous to water is seldom reported in the literature [22,23]. In the case of glasses, the properties of iron phosphate and borosilicate glasses have been compared [24], and iron phosphate glasses exhibited better chemical durability in water at 90 °C than borosilicate glasses. The substitution of phosphorous with iron in the P—O—P bonds can explain this better resistance to hydration. However, these glasses are very sensitive to water because the P—O—P bonds hydrolyze easily. Thus, incorporation of water in the form of —OH groups must be considered as a network modification [25]. Few references on the water resistance of geopolymers are available. However, Ilkentar et al. [26] noted that in the case of an alkali-activated fly ash geopolymer, the water absorption of the material tended to increase with the setting temperature. However, the samples immersed in water leached alkali ions, which do not react [27].

The objective of this work was to identify the most favorable experimental conditions for processing geopolymers in an acidic medium (phosphoric acid), which are closely linked to the structures formed from several metakaolin raw materials that are already commonly used in basic media [7]. As few scientific studies have focused on the water and thermal resistances of acidic geopolymers, thermal and water resistance tests completed by thermal and structural analyses were performed to determine the most effective formulation.

2. Experimental details

2.1. Raw materials

Three types of aluminosilicate sources supplied by Imerys were used in this study (Table 1). Denoted M1, M3 and M4, the sources have been characterized by Gharzouni et al. [7]. M1 and M4 had already been heat-treated by the supplier, whereas M3 was obtained from the transformation of initially supplied kaolin in metakaolin after thermal treatment at 750 °C for 4 h (heating rate of 5 °C/min). The phosphoric acid used in the study was an 85 wt% phosphoric acid solution supplied by VWR with a concentration of 14.7 mol.L^{-1}. Consolidated materials were synthesized (experimental procedure illustrated in Fig. 1) by mixing the metakaolin materials with diluted phosphoric acid solutions to obtain different Al/P molar ratios (Al/*P* = 1 and 4) and concentrations of phosphoric acid to prepare consolidated materials. The different Al/P, Al/H_2O and Al/Si ratios used are reported in Table 2. The obtained mixtures were placed in a sealable polystyrene mold at different temperatures (20 °C, 40 °C and 70 °C). Samples with typical dimensions of 15 mm in diameter and 30 mm in height are denoted x-My-T, where x represents the Al/P ratio, My represents the metakaolin source, and T represents the consolidation temperature of the samples. All samples names are compiled in Table 3.

Table 1
Physical and chemical properties of the raw metakaolins. [1]

Metakaolin	Si/Al	d50 (μm)	BET value (m^2/g)	Wettability (μL/g)	Amorphous phase (%) [1]	Heating process
M1	1.17	10.0	17	760	63	Rotary
M3	1.00	8.0	8	1010	98	Oven
M4	0.98	6.0	17	1186	98	Flash

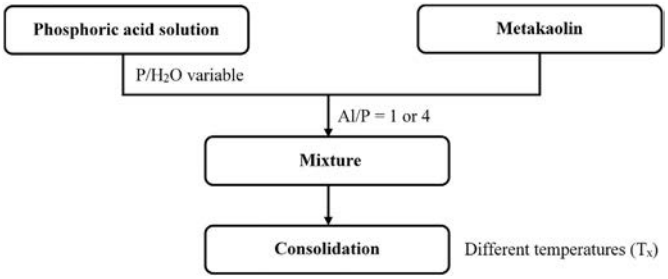

Fig. 1. Synthesis protocol of samples.

2.2. Sample characterization

The setting time is defined as the moment when the geopolymer can sustain manipulation without any deformation [28]. Consolidation was checked every hour the first day after preparation and then every 12 h each following day.

Consolidated samples were immersed in water after 7 days at an liquid/solid ratio equal to 1. The external visual aspect of the samples was observed after 7 days of static immersion in water: if coarse cracks or disaggregations could be observed on a specimen, the specimen was

Table 2:
Al/P, Al/H_2O and Al/Si ratios used for different compositions.

Samples	Al/P	Al/H_2O	Al/Si
1-M1-20	1	0.62	0.85
1-M1-40	1	0.62	0.85
1-M1-70	1	0.62	0.85
1-M3-20	1	0.41	1.00
1-M3-40	1	0.41	1.00
1-M3-70	1	0.41	1.00
1-M4-20	1	0.27	1.02
1-M4-40	1	0.27	1.02
1-M4-70	1	0.27	1.02
4-M1-20	4	0.23	0.85
4-M1-40	4	0.23	0.85
4-M1-70	4	0.23	0.85
4-M3-20	4	0.19	1.00
4-M3-40	4	0.19	1.00
4-M3-70	4	0.19	1.00
4-M4-20	4	0.15	1.02
4-M4-40	4	0.15	1.02
4-M4-70	4	0.15	1.02

Table 3:
Nomenclature of the studied samples and their consolidated temperature at ambient pressure.

Samples	Al/P	Metakaolin	Temperature (°C)
1-M1-20	1	M1	20
1-M1-40	1	M1	40
1-M1-70	1	M1	70
1-M3-20	1	M3	20
1-M3-40	1	M3	40
1-M3-70	1	M3	70
1-M4-20	1	M4	20
1-M4-40	1	M4	40
1-M4-70	1	M4	70
4-M1-20	4	M1	20
4-M1-40	4	M1	40
4-M1-70	4	M1	70
4-M3-20	4	M3	20
4-M3-40	4	M3	40
4-M3-70	4	M3	70
4-M4-20	4	M4	20
4-M4-40	4	M4	40
4-M4-70	4	M4	70

classified into the 0% group, whereas if no defect was visible, the specimen was classified into the 100% category. Intermediate cases occurred when slight defects were observed (denoted the 50% group).

The experimental procedure used to characterize thermal resistance consists in heating each specimen to 1000 °C (ramp rate of 5 °C/min, dwell time of 2 h and natural cooling) in a furnace. Similarly to water resistance, thermal resistance was evaluated according to visual aspect (possible occurrence of cracks or melted areas). At least three specimens submitted to the same conditions were characterized to ensure the reproducibility of the setting time, water resistance and thermal resistance results.

The samples were examined by X-ray diffraction (XRD) on a Brüker D8 Advance diffractometer using CuK_{α} radiation. The data were collected over a 2θ angular range of 5–60° with a step size of 0.02° and an equivalent measured time per step of 50 s. The crystalline phases were identified from the experimental patterns using the powder diffraction file (PDF) database of the International Center for Diffraction Data. The positions of the amorphous bands present in the diagrams were determined using Peakoc software [29] with a precision of 0.01°. A Voigt function was used to model the peaks belonging to crystalline phases, while a simpler Gaussian function was used for the amorphous bands. A linear function was chosen to account for the background, and the $K_{\alpha 1}$-$K_{\alpha 2}$ doublet was considered. All of these analyses were performed over the 2θ range 10–40° via a two-step process. First, the profile parameters of the peaks originating from the crystalline phases were refined. Then, the same procedure was performed for the amorphous contributions while holding the parameters of the crystalline phases constant.

Differential thermal analysis (DTA) and thermogravimetric analysis (TGA) were performed with an SDT Q600 apparatus from TA Instruments in an atmosphere of flowing dry air (100 mL/min) in platinum crucibles. The signals were measured with Pt/Pt–10%Rh thermocouples. The samples were heated to 1000 °C at a rate of 5 °C/min.

Compressive strength measurements were performed with a LLOYD EZ20 universal testing machine with a crosshead speed of 0.5 mm/min. Measurements were conducted five times for each composition on cylindrical samples (15 mm in diameter and 30 mm tall) previously stored at room temperature in a closed mold for 7 days. The reported compressive strength value (MPa) is the average of the five measurements.

The morphologies of the samples were observed using an FEI Quanta FEG 450 scanning electron microscope (SEM). A carbon layer of 18 nm was deposited by evaporation on the samples before observation.

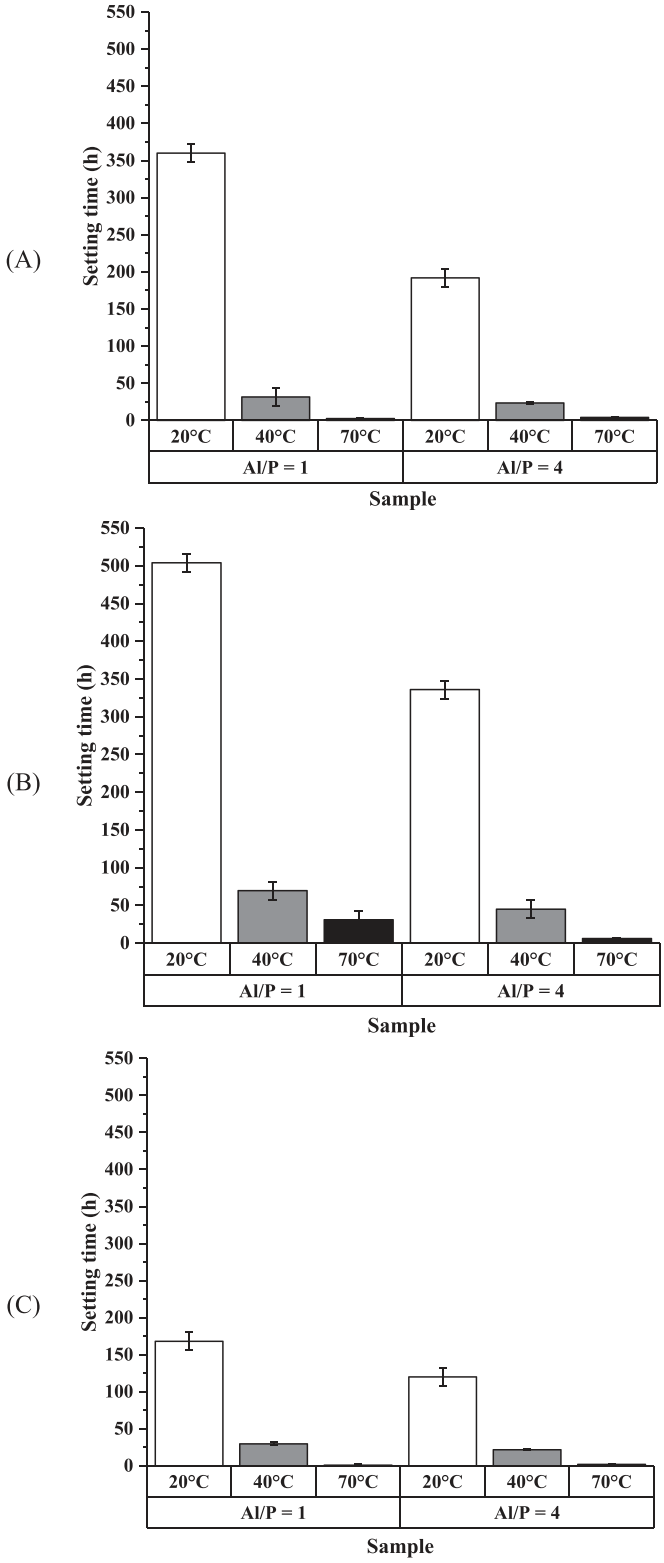

Fig. 2. Setting time of Al/P = 1 and 4 samples with (A) M1, (B) M3 and (C) M4 for (□) 20°C, (■) 40°C and (■) 70°C.

3. Results

3.1. Fresh samples

The results obtained at the different setting times for M1, M3 and M4 at Al/P ratios of 1 and 4 and at different temperatures (20, 40,

70 °C) are shown in Fig. 2. For metakaolin M1, the setting time increases as the temperature decreases regardless of the Al/P ratio. Therefore, an increase in the Al/P ratio reduces the setting time of the samples. The geopolymers synthesized with M3 and M4 show the same trend. However, the kinetics vary with the type of metakaolin used. For instance, for the samples formed at 20 °C with a Al/P ratio of 1, the geopolymer synthetized with M4 is the first to consolidate followed by that synthesized with M1 and finally with M3. An increase in temperature throughout the consolidation of the samples reduces the setting time. This increase induces thermal agitation of the molecules in the sample, which facilitates the dissolution of the species. The polycondensation reactions are then promoted, which results in faster consolidation kinetics. The geopolymers with an Al/P ratio of 1 exhibit the same proportions of phosphorus, aluminum and silicon, leading to the formation of secondary phases due to the occurrence of various interactions. Therefore, the setting time increases with an increase in the Al/P ratio to 4. Samples with this ratio contain an excess of silicon and aluminum, and consequently, different networks are created, inducing metastable phases, as evidenced in basic geopolymers [30]. This behavior can be correlated to the use of metakaolin materials with different Si/Al ratios [31]. In effect, the aluminosilicate sources M1, M3 and M4 have successively, different Si/Al ratios (1.17, 1.00 and 0.98, respectively) (Table 1). Moreover, they display also wettability and amorphous rate in agreement with tetrahedral aluminum which permit to classify in the following reactivity order: M4 ≥ M3 ≥ M1. Metakaolin M4, the most reactive without impiruty according to Gharzouni et al. [7], quickly releases aluminum and silicon, which are then able to react with phosphorous species. The M3 metakaolin of lower wettability and reactivity is able to release the species but the kinetic is lower. Finally, the M1 metakaolin containing impurities (quartz, mica) with a weak amorphous rate releases the Al and Si very slowly.

With M4, the aluminum, which is the limiting species, can react with phosphorous, and the presence of excess of phosphorous leads to the formation of metastable phases, inducing a short consolidation time. These metastable phases are composed of unreacted phosphorous and silicon and amorphous hydrates. In the presence of the less reactive metakaolin M1, the release of aluminum and silicon is slow and is further delayed by the presence of micas. This slow release delays the various reactions, and secondary phases form in competition with mica. These secondary phases formed from the metakaolin with a slow dissolution ability consist of silicon and aluminum hydrates that can surround the mica plates. This explanation is in agreement with the fact that the M1-based samples display longer setting times than do the M4-based samples. Metakaolin M3 is the least reactive among the three sources, although the species are mobile due to their wettability. In this case, various exchanges are facilitated by the initiating reactions, concordant with the setting time observed for the geopolymers.

The results of the mechanical compression tests are shown in Fig. 3 (examples of the observed behavior) and Table 4. The 1-M1-70 and 1-M4-70 samples could not be examined: the initial dimensions were strongly affected by the setting temperature; thus, the geometry of the specimens was no longer compatible with the required experimental equipment. Based on the values of stress to rupture, nearly all the samples synthesized with an Al/P ratio of 1 (except for the 1-M3-20 sample) yield compressive stress values ranging from 44 to 110 MPa. Among these samples, those prepared with different metakaolin materials (M1, M3 and M4) at 20 °C exhibit different mechanical behaviors. Specifically, the materials with metakaolins M1 and M4 exhibit brittle rupture (conventional, almost linear stress-strain law behavior with sudden catastrophic fracture without any plastic deformation), with small elastic deformation (systematically lower than 3%). By contrast, the sample containing M3 exhibits non-conventional behavior because a substantial plastic deformation step (up to 50%) occurs before failure at a very low level of stress. For metakaolin M1, the compressive stress increases with the temperature of consolidation. This phenomenon is also observed with metakaolins M3 and M4. This trend can be explained by greater cohesion in the material because

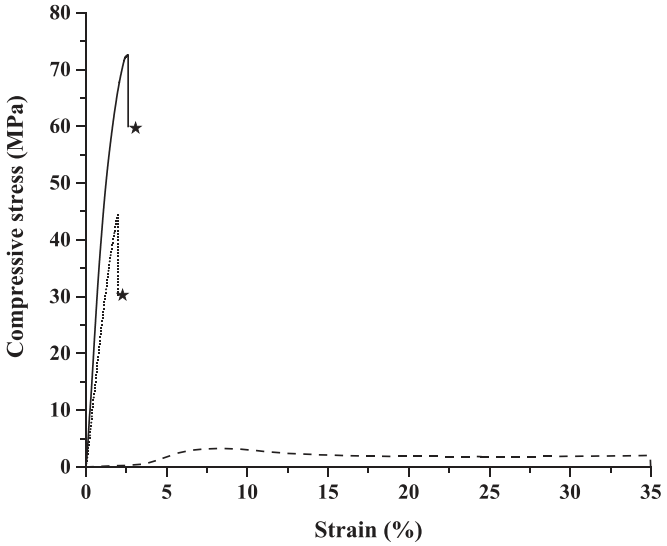

Fig. 3. Compressive stress value in function of strain (★ rupture) for 1-M1-20 (—), 1-M3-20 (—) and 1-M4-20 (…) samples.

Table 4:
Maximal stress value (σ_{cmax}) and mechanical behavior under compressive loading for all tested specimens (BR: Brittle Rupture/Low strain to rupture value < 3% and PD: Plastic deformation/High strain to rupture value > 10%).

Samples	σ_{cmax}(MPa)	Mechanical behavior	Groups
1-M1-20	73	BR	TR
1-M1-40	110	BR	TR
1-M1-70	–	–	TR
1-M3-20	3	PD	TR
1-M3-40	86	BR	TR
1-M3-70	90	BR	WR1
1-M4-20	44	BR	WR1
1-M4-40	60	BR	WR1
1-M4-70	–	–	WR1
4-M1-20	3	BR	N
4-M1-40	3	BR	N
4-M1-70	2	BR	N
4-M3-20	2	PD	WR2
4-M3-40	0	BR	N
4-M3-70	2	BR	WR2
4-M4-20	2	BR	WR2
4-M4-40	2	BR	N
4-M4-70	1	BR	N

thermal agitation of the molecules in the sample facilitates the dissolution of the species that promotes the polycondensation reaction. In addition, the samples containing M1 exhibit higher mechanical performance than that of the samples containing M3 and M4. With increasing Al/P ratio, the compressive stress at fracture decreases significantly (< 5 MPa). The samples 1-M1-70 and 1-M4-70 formed at higher temperatures exhibit a higher compressive stress, as expected. With an Al/P ratio equal to 1, secondary phases are created due to various interactions, and these phases induce strengthening of the compressive stress over that of the samples with an Al/P ratio of 4, as this ratio results in metastable phases detrimental to high compressive stress values.

The consolidated samples and the results of water and thermal resistance tests are shown in Table 5 for each metakaolin with an Al/P ratio of 1 and a setting temperature of 20 °C. All samples are systematically consolidated regardless of the type of used metakaolin. The water resistance is observed macroscopically. The sample incorporating M1 cracked in water following water infiltration in the sample. Water with M3 sample became trouble following the disaggregation of sample. In contrast, the samples made from M4 were resistant to water. However, the opposite trend was observed for the thermal resistance.

Table 5:
Example of consolidated materials and their water and thermal resistance tests for 1-M1-20, 1-M3-20 and 1-M4-20 samples.

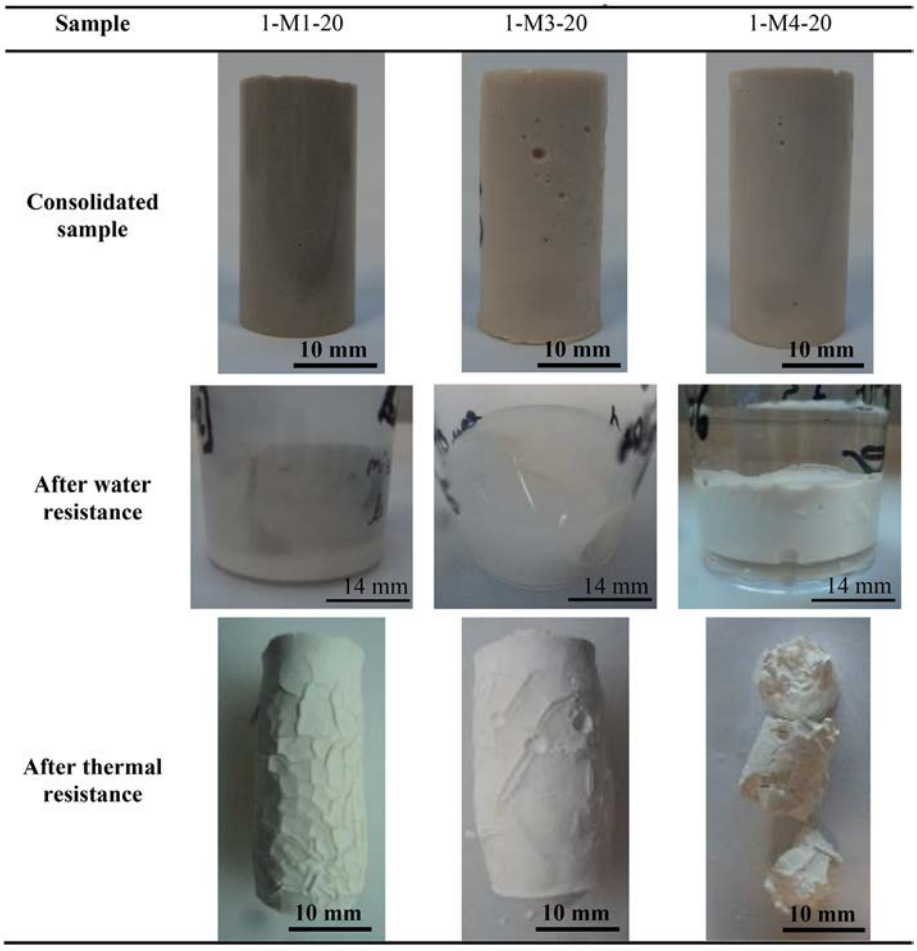

The samples synthesized with M1 and M3 did not break after thermal treatment, while those synthesized with M4 did. After thermal resistance tests, samples showed volume expansion or volume shrinkage rates ranging from +33% to −21%. For the three samples reported in Table 5, an expansion is noted for 1-M1-20 and 1-M3-20 (33% and 1% respectively), whereas the shrinkage of 1-M4-20 is approximately −19%. Thus, samples with high thermal resistance expanded with temperature, whereas the others shrank after heat treatment at 1000 °C.

The water and thermal resistances of the samples containing M1, M3 and M4 and with an Al/P ratio of 1 or 4 are presented in Fig. 4. The samples containing M1 do not resist water immersion regardless of the Al/P ratio or setting temperature. For the Al/P ratio of 1, the samples are thermal resistant irrespective of the applied setting temperature. However, with increasing Al/P ratio, the samples become brittle after heat treatment. With M3 and an Al/P ratio equal to 1, the samples consolidated at 20 °C and 40 °C are not water resistant, but they are thermal resistant. The reverse behavior is observed for the sample consolidated at 70 °C. For an Al/P ratio equal to 4, the samples consolidated at 20 °C and 70 °C are resistant to water, unlike the sample consolidated at 40 °C. None of the samples are resistant to fire, regardless of the temperature applied. The metakaolin M4 produces samples with the opposite behavior of those formed with M1 for an Al/P ratio equal to 1. For all temperatures and an Al/P ratio equal to 1, the geopolymers are resistant to water but not heat. For an Al/P ratio equal 4, the samples consolidated at 20 °C have similar properties to those with an Al/P ratio equal to 1. However, the samples consolidated at 40 °C and 70 °C are not resistant to water.

All these data indicate that three types of materials are produced. Four different groups can then be distinguished from the different samples. The first group, named TR for thermal resistance, is resistant to temperature but not water. The second and third groups, named WR1 (Al/P = 1) and WR2 (Al/P = 4) for water resistance, contain samples that are water resistant but not fire resistant. The two Al/P ratios present in this group suggest the possibility of subgroups. Samples that are neither water nor thermal resistant belong to the last group, called N for none. The mechanical properties of each group are summarized in Table 4.

3.2. *Behavior of the four groups*

The four families are now examined with a focus on the characteristics of one sample from each family. 1-M1-20, 1-M4-70, 4-M4-20 and 4-M4-70 samples are chosen as representatives of the TR, WR1, WR2 and N families, respectively. The XRD patterns of each sample were measured, and the crystalline phases were identified. Selected patterns of the geopolymers prepared from each metakaolin with Al/P = 1 and Al/P = 4 and different setting temperatures are presented in Fig. 5.A. For comparison, the XRD pattern of metakaolin M1 is also shown. Metakaolin M1 is composed of an amorphous part, as indicated by the broad band observed at approximately 20°, and crystalline impurities that were present in the original kaolin and maintained after calcination. These impurities are identified as well-crystallized quartz (PDF n°. 00-046-1045), muscovite (PDF n°. 00-003-0849) and anatase (PDF n°. 01-071-1166). The geopolymer 1-M1-20 has a comparable XRD pattern, and thus, the crystalline impurities in this sample are the

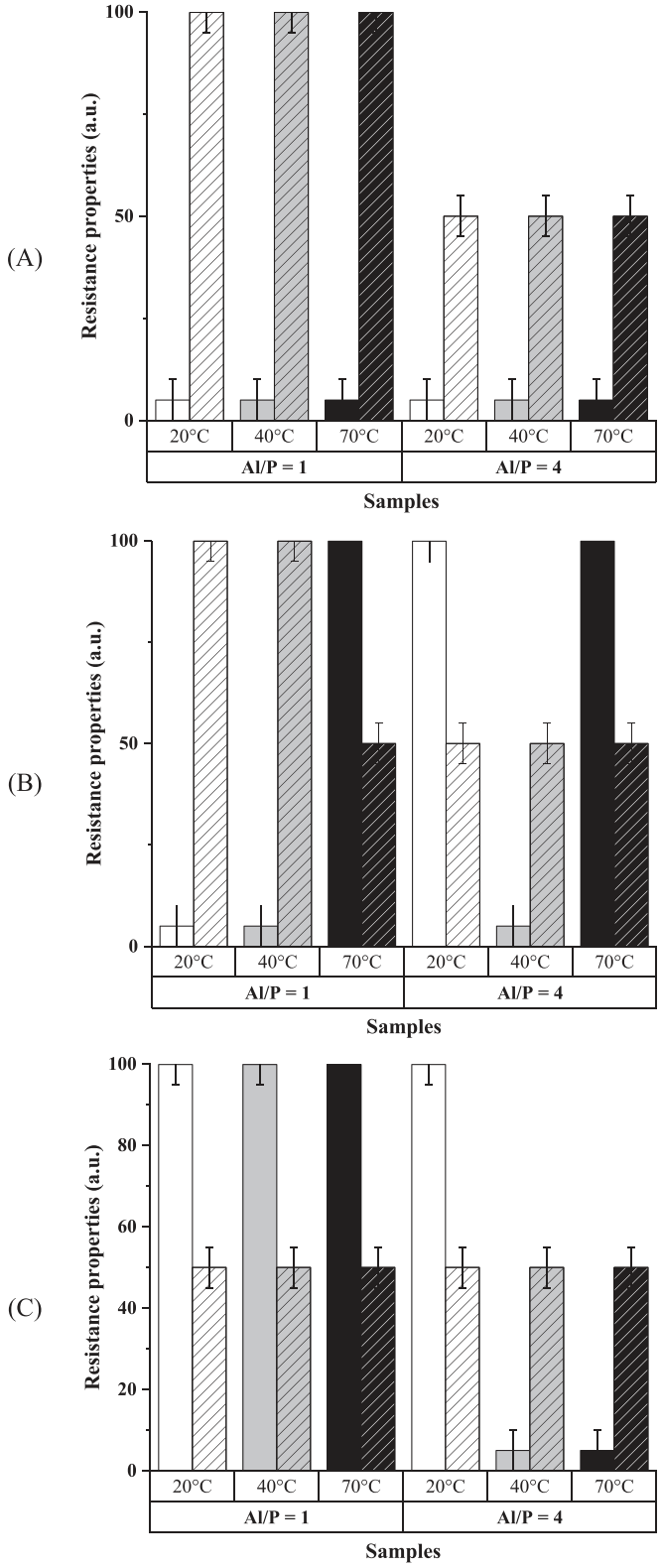

Fig. 4. Water (empty area) and thermal (hatched area) resistance properties of Al/P = 1 and 4 samples with (A) M1, (B) M3 and (C) M4 for (□) 20°C, (■) 40°C and (■) 70°C.

same as those in the metakaolin, although the intensities of the muscovite peaks are lower, indicating a change in this phase. The band from the amorphous phase is more intense than that of the metakaolin and is shifted towards larger angles. The same trend occurs with the

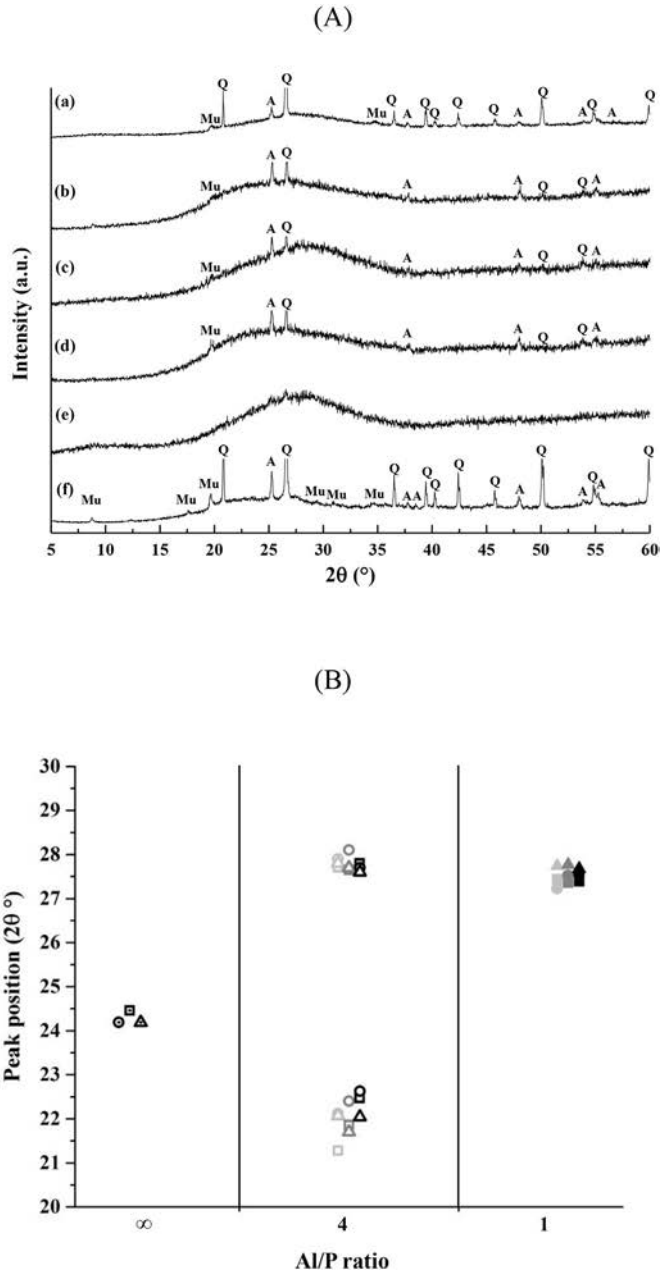

Fig. 5. (A) Xray diagrams of (a) 1-M1-20 [TR], (b) 4-M4-70 [N], (c) 1-M4-70 [WR1], (d) 4-M4-20 [WR2] and (e) 1-M3-20 samples and the metakaolin (f) M1 and (B) refined positions of the amorphous domes present in the metakaolins (□) M1, (○) M3 and (Δ) M4, and in Al/P = 1 samples for 1-Mx-Ty (filled symbol) and Al/P = 4 samples 4-Mx-Ty (empty symbol) for x = (■) 1, (●) 3, (▲) 4 and y = (■) 20, (■) 40, (■) 70.
Q: crystallized quartz (PDF n°00-046-1045), Mu: muscovite (PDF n°00-003-0849) and A: anatase (PDF n°01-071-1166).

geopolymers prepared from metakaolin M4 where the position of the amorphous band shifts towards larger angles. The patterns of geopolymers 4-M4-70 and 4-M4-20 are very similar to those of the 1-M4 family of geopolymers with the exception of the position and intensity of the amorphous band. Finally, the pattern of M3 is even simpler, as no crystalline impurities are identified in the metakaolin or the geopolymer (see the example provided for 1-M3-20). Only displacement of the amorphous band with different Al/P ratios is observed. For all the samples, no clear influence of the consolidation temperature on the crystalline impurities or the position of the amorphous band is observed.

The positions of the amorphous bands were then refined using the Peakoc program. The amorphous dome of metakaolin and the samples with Al/P = 1 were fitted using a single peak, while those of the samples with Al/P = 4 needed a second low intensity peak at approximately 22° to achieve a suitable fit. The refinement results are presented in Fig. 5.B. The peak positions of the pure metakaolins are very similar, which confirms the similar structures of these materials despite their slightly different compositions. For the Al/P = 1 samples, the peak is clearly shifted towards larger angles, and the new position does not seem to be influenced by the starting metakaolin or the consolidation temperature. This new position with an average value of 27.52° is characteristic of the new amorphous network formed in the geopolymer and can be related to the most intense peak from the $AlPO_4$ phase. For the Al/P = 4 compositions, the results again are not clearly influenced by the metakaolin or the consolidation temperature. The same intense band is found at an average position of 27.77°, and a low-intensity band is observed at approximately 22°. The position of this band clearly differs from that of starting metakaolin showing that the original network is modified by the reaction with phosphoric acid. These results indicate that for the Al/P = 4 compositions, the geopolymerization process is not complete due to the lack of sufficient PO_4^{3-} units, and the final amorphous network is not present in the full sample.

Fig. 6 shows four different microstructures of the fresh samples. The samples based on an Al/P ratio equal to 1 display a homogeneous microstructure with some cracks formed from their poor mechanical properties. In contrast, an increase in the ratio Al/P produces another microstructure that is porous and has various particle sizes. More precisely, the 1-M1-20 sample exhibits a microstructure similar to that of a previously reported geopolymer [32], in agreement with the thermal resistance properties. An increase in the synthesis temperature leads to the formation of a microstructure (1-M4-70) consisting of encapsulated particles, revealing a fast setting process that includes the unreacted particles. This microstructure can explain the water resistance of the sample since no pores appear on the surface [33]. Finally, the 4-M4-20 and 4-M4-70 samples display heterogeneous and disordered microstructures due to their non-stoichiometric molar ratio. However, some differences are notable, such as the presence of spherical particles in the 4-M4-70 sample, which are indicated by circles (○) in Fig. 6. This feature could be responsible for the lack of resistance in comparison with sample 4 -M4-20. In addition, a temperature of 70 °C produces some strain in the sample, leading to a different structure with no thermal resistance.

The mass loss and heat flow curves of the four samples are presented in Fig. 7. The mass loss related to the loss of water present in the samples occurs between 50 and 250 °C, and the total weight loss consists of between 25 and 45% water. The mass loss of the samples with an Al/P ratio equal to 1 is lower than that of the samples with an Al/P ratio of 4. Sample 1-M1-20 contains less water than 1-M4-70, and 4-M4-20 possess slightly more water than 4-M4-70 due to its lower consolidation temperature. In general, larger mass losses are observed between 25 and 200 °C. These losses are associated with endothermic peaks related to water loss from the reaction mixture and to various polycondensation reactions. Specifically, for the samples that exhibit thermal resistance, such as 1-M1-20, two-stage water loss is observed with low endothermic peaks. The values of these peaks are close to those obtained from the polycondensation reactions under basic

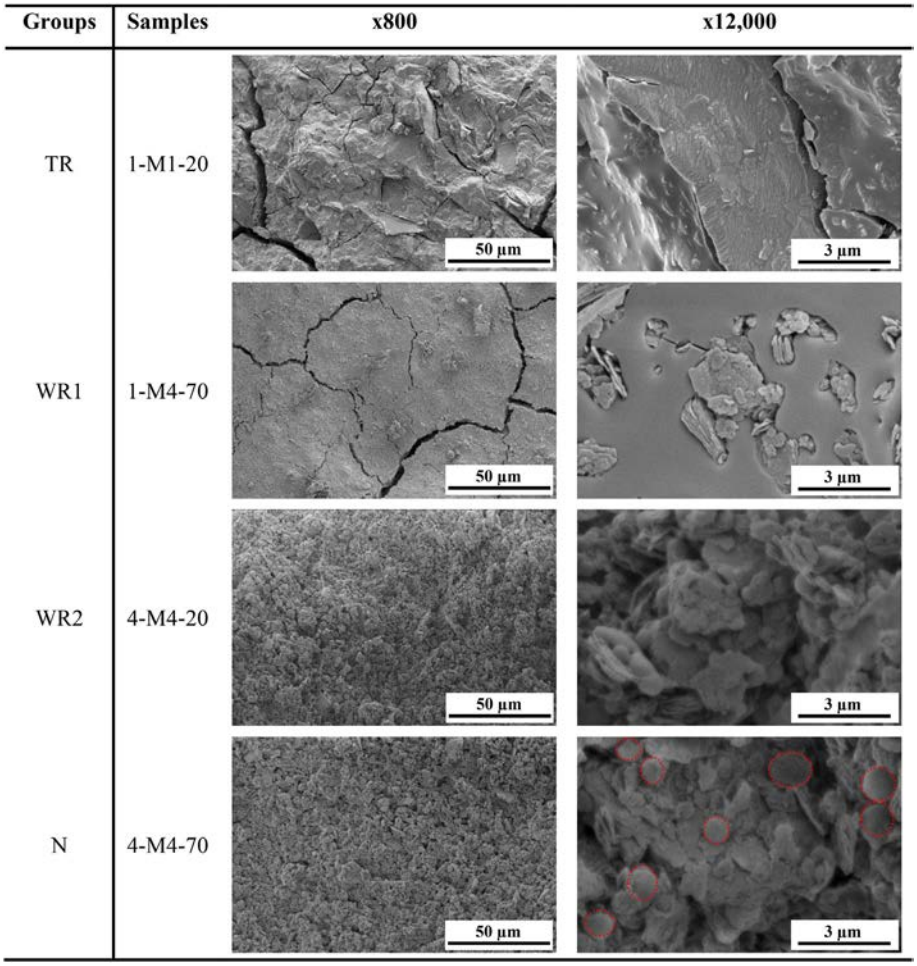

Fig. 6. SEM photo of various samples, ○ spherical particles.

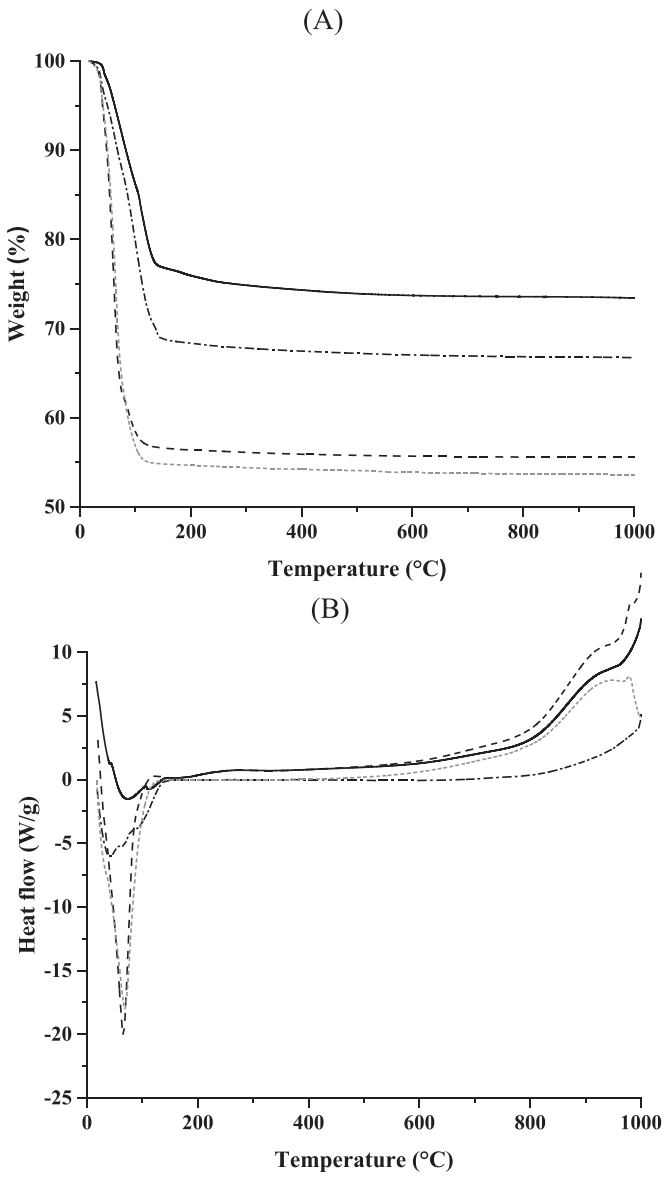

Fig. 7. (A) Weightloss and (B) heat flow curves of (—) TR sample 1-M1-20, (-.-.-) WR1 sample 1-M4-70, (…) WR2 sample 4-M4-20 and (—) N sample 4-M4-70.

conditions [21]. For 1-M4-70, which is a water-resistant sample, a larger amount of water is present in the sample, highlighting the presence of strong interactions formed by the polycondensation reactions, in agreement with the metastable phases. As the temperature increases, consolidation-induced thermal agitation makes the material more unstable. Indeed, the reactions are hindered, which decreases the strength, as in the previously reported glasses [34]. In this case, the transition to the vitreous phases is consistent with the observed resistance to water but not fire. For an Al/P ratio equal to 4, different reactions occur due to the difference in stoichiometry. The water losses are greater for these samples due to the formation of metastable phases and the occurrence of various polycondensation reactions that promote disorder and the formation of pores, thus leading to a decrease in temperature [35], [36]. The large amount of water present in 4-M4-70, which is not resistant to water or fire, leads to the same behavior but with added constraints due to the higher temperature. When the reactions produce stable compounds, water resistance is imparted, as found for sample 4-M4-20.

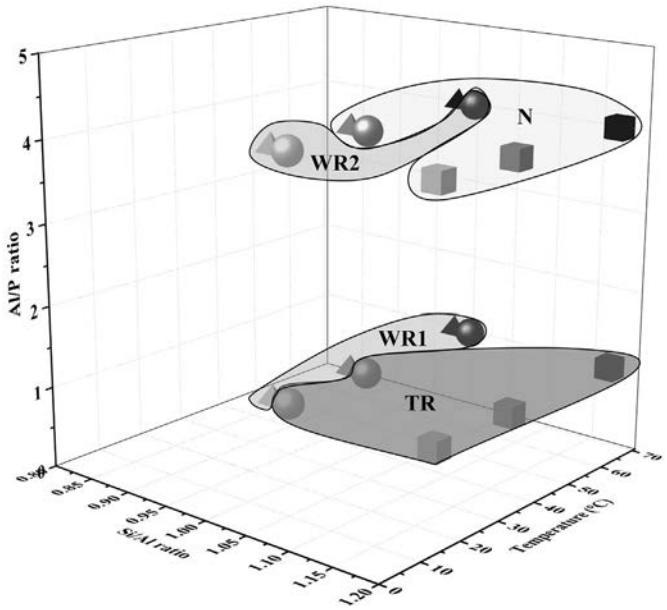

Fig. 8. Resistance properties in function of the Si/Al, Al/P ratios and the temperature for 1-Mx-Ty and 4-Mx-Ty with x = (■) 1, (●) 3, (▲) 4 and y = (■) 20, (■) 40, (■) 70.

4. Discussion

To understand the various behaviors observed for the four types of samples, Fig. 8 shows all the compositions as a function of the Si/Al ratio, Al/P ratio and setting temperature. The four highlighted areas correspond to the groups defined as TR, WR1, WR2 and N. The TR family corresponds to samples with an Al/P ratio equal to 1 a Si/Al ratio greater than or equal to 1 and a temperature of 20 or 40 °C. These conditions lead to the formation of secondary phases in relation to the two metakaolins (M1 and M3). An increase in temperature does not dramatically change the TR sample with the exception of 1-M1-70, in which the increase of temperature favors dissolution, and consequently, these samples display resistance behavior.

Water resistance is observed for the samples with a Si/Al ratio less than or equal to 1 and either Al/P ratio. This behavior is strongly dependent on the consolidation temperature. For an Al/P ratio equal to one, the dissolution of metakaolin must be low to induce polycondensation, leading to a closed network like that of a glass. As an example, the 1-M4-T_x (x = 20, 40, 70 °C) and 1-M3-70 samples are water resistant while 1-M3-20 and 1-M3-40 are not. In these two samples, the low temperatures do not facilitate the formation of consolidated materials in which polycondensation is favorable. An increase in the Al/P ratio to four leads to the formation of a water-resistant material when the silicate, phosphate and aluminum species are able to react to form metastable phases that prevent water diffusion. As previously demonstrated, the other samples do not display desirable properties.

More precisely, Fig. 9 shows the variations in the maximum compressive stress and the mass loss of all the samples as a function of the number of moles of aluminum in the samples. As previously mentioned, the four families can be distinguished. Moreover, the amount of water decreases with the quantity of reactive aluminum. Samples with an Al/P ratio equal to four contain less aluminum than those with Al/P = 1. In addition, the samples that exhibit the highest compressive stress values contain lower amounts of water (between 25 and 29%) and > 0.17 mol of Al, leading to thermal resistance. For the samples containing an aluminum content between 0.14 and 0.17 mol, the mechanical properties remain acceptable, and the samples are water resistant. For an aluminum content < 0.14 mol, the sample exhibits a lower compressive

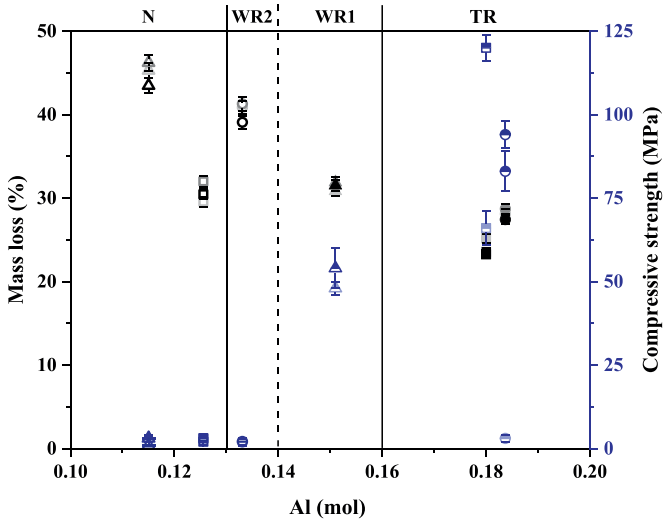

Fig. 9. Variation of the maximal compressive stress (blue symbol) and the mass loss (black symbol) in function of reactive aluminium for 1-Mx-Ty (filled symbol) and 4-Mx-Ty (empty symbol) for x = (■) 1, (●) 3, (▲) 4 and y = (■) 20, (■) 40, (■) 70.

strength. Consequently, these data underline the possibility that the aluminum content determines the mechanical properties.

5. Conclusion

The aim of this paper was to examine the effect of the chemical composition on the thermal and fire resistance of compounds with acceptable mechanical properties in relation to the setting time, which depends on the consolidation temperature. The various data obtained from thermal analysis, SEM measurements, and XRD have shown the existence of four types of compounds. All these data can be summarized as a function of the Al/P and Si/Al ratios and the mechanical properties and as a function of the quantity of aluminum.

(i) The TR samples correspond to an aluminum content > 0.17 and a compressive strength above 54 MPa.
(ii) For the WR samples, the WR1 samples possess an aluminum content between 0.14 and 0.17 and a compressive strength between 48 and 54 MPa, whereas the WR2 samples possess an aluminum content between 0.13 and 0.14 and a compressive strength below 5 MPa.
(iii) The N samples contain an aluminum content below 0.13 and a compressive strength below 5 MPa.

This work has permitted us to highlight the different amounts of aluminum element contained in acid geopolymers required to achieve certain mechanical properties and water or thermal resistance.

References

[1] J. Davidovits, Geopolymer: Chemistry and Applications, second ed, Geopolymer institute, Saint-Quentin, France, 2008.
[2] J. Davidovits, Geopolymers, J. Therm. Anal. 37 (8) (1991) 1633–1656.
[3] H. Xu, Geopolymerisation of Aluminosilicate Minerals, PhD Thesis, Department of Chemical Engineering, University of Melbourne, Australia, 2001.
[4] M.W. Grutzeck, D.D. Siemer, Zeolithes Synthesised from Class F Fly Ash and Sodium Aluminate Slurry, J. Am. Ceram. Soc. 80 (9) (1997) 2449–2458.
[5] H. Rahier, J. Wastiels, M. Biesemans, R. Willem, G. Van Assche, B. Van Mele, Reaction mechanism, kinectics and high temperature transformations of geopolymers, Mater. Sci. 42 (2007) 2982–2996.
[6] P. Duxson, A. Fernandez-Jimenez, J.L. Provis, G.C. Lukey, A. Palomo, J.S.J. Van Deventer, Geopolymer technology: the current state of the art, J. Mater. Sci. 42 (2007) 2917–2933.
[7] A. Gharzouni, Contrôle de l'attaque des sources aluminosilicates par la comprehension des solutions alcalines, PhD Thesis, Université de Limoges et de Sfax, 2016.
[8] X.X. Gao, A. Autef, E. Prud'homme, P. Michaud, E. Joussein, S. Rossignol, Synthesis of consolidated materials from alkaline solutions and metakaolin: existence of domains in the Al–Si–K/O ternary diagram, J. Sol-Gel. Sci. Tech. 65 (2) (2013) 220–229.
[9] A. Gharzouni, I. Sobrados, E. Joussein, S. Baklouti, S. Rossignol, Predictive tools to control the structure and the properties of metakaolin based geopolymer materials, Colloids Surf. A Physicochem. Eng. Asp. 511 (2016) 212–221.
[10] H.K. Tchakouté, C.H. Rüscher, Mechanical and microstructural properties of metakaolin-based geopolymer cements from sodium waterglass and phosphoric acid solution as hardeners: a comparative study, Appl. Clay Sci. 140 (2017) 81–87.
[11] S. Louati, S. Baklouti, B. Samet, Acid based geopolymerization kinetics: effect of clay particle size, Appl. Clay Sci. 132-133 (2016) 571–578.
[12] H. Douiri, S. Louati, S. Baklouti, M. Arous, Z. Fakhfakh, Structural, thermal and dielectric properties of phosphoric acid-based geopolymers with different amounts of H_3PO_4, Mater. Lett. 116 (2014) 9–12.
[13] D.S. Perera, J.V. Hanna, J. Davis, M.G. Blackford, B.A. Latella, Y. Sasaki, E.R. Vance, Relative strengths of phosphoric acid-reacted and alkali-reacted metakaolin materials, J. Mater. Sci. 43 (2008) 6562–6566.
[14] L. Xu, C. Lei, R. Xu, X. Zhang, F. Zhang, Synergistic effect on flame retardancy and thermal behavior of polycarbonate filled with α-zirconium phosphate@gel-silica, J. Appl. Polym. Sci. 44829 (2017).
[15] J.-M. Chiou, D.D.L. Chung, Improvement of the temperature resistance of aluminium-matrix composites using an acid phosphate binder, J. Mater. Sci. 28 (1993) 1471–1487.
[16] D. Jianng, M. Pan, X. Cai, Y. Zhao, Flame retardancy of rice straw-polyethylene composites affected by *in situ* polymerization of ammonium polyphosphate/silica, Compos. Part A 109 (2018) 1–9.
[17] L. Yang, Z. Xu, X. Wang, Influence of nano-silica on the flame retardancy and smoke suppresion properties of transparent intumescent fire-retardant coatings, Prog. Org. Coat. 112 (2017) (319–239).
[18] S.A. Bernal, J. Bejarano, C. Garzón, R.M. de Gutiérrez, S. Delvasto, E.D. Rodríguez, Performance of refractory aluminosilicate particle/fiber-reinforced geopolymer composites, Compos. Part B 43 (2012) 1919–1928.
[19] A. Sabbatini, L. Vidal, C. Pettinari, I. Sobrados, S. Rossignol, Control of shaping and thermal resistance of metakaolin-based geopolymers, Mater. Des. 116 (2017) 374–385.
[20] M. Sarkar, K. Dana, S. Das, Microstructural and phase evolution in metakaolin geopolymers with different activators and added aluminosilicate fillers, J. Mol. Struct. 1098 (2015) 1110–1180.
[21] S.A. Bernal, D.E. Rodri'guez, R.M. de Gutie'rrez, M. Gordillo, J.L. Provis, Mechanical and thermal characterization of geopolymers based on silicate-activated metakaolin/slag blends, J. Mater. Sci. 46 (2011) 5477–5486.
[22] Y. Tan, Y. Liu, L. Grover, Effect of phosphoric acid on the properties of magnesium oxychloride cement as a biomaterial, Cem. Concr. Res. 56 (2014) 69–74.
[23] Y. Jin, L. Xiao, F. Luo, Influence of fly ash on the properties of magnesium oxychloride cement, Adv. Mater. Res. 662 (2013) 406–408.
[24] D.E. Day, Z. Wu, C.S. Ray, P. Hrma, Chemically durable iron phosphate glass wasteforms, J. Non-Cryst. Solids 241 (1998) 1–12.
[25] D. Brauer, D. Möncke, RSC Smart Materials 23 – Chapter 3 Introduction to the Structure of Silicate, Phosphate and Borate Glasses, (2017).
[26] S. İlkentapar, C.D. Atiş, O. Karahan, E.B. Görür Avşaroğlu, Influence of duration of heat curing and extra rest period after heat curing on the strength and transport characteristic of alkali activated class F fly ash geopolymer mortar, Constr. Build. Mater. 151 (2017) 363–369.
[27] W.D.A. Rickard, C.D. Borstel, A. Riessen, The effect of pre-treatment on the thermal performance of fly ash geopolymers, Thermochim. Acta 573 (2013) 130–137.
[28] H. Celerier, J. Jouin, V. Mathivet, N. Tessier-Doyen, S. Rossignol, Composition and properties of phosphoric acid-based geopolymers, J. Non-Cryst. Solids 493 (2018) 94–98.
[29] O. Masson, PEAKOC Profile Fitting Software v1.0, (2006) (access at).
[30] A. Autef, E. Joussein, A. Poulesquen, G. Gasnier, S. Pronier, I. Sobrados, J. Sanz, S. Rossignol, Role of metakaolin purities on potassium geopolymer formulation: the existence of several networks, J. Colloid Interface Sci. 408 (2013) 43–53.
[31] A. Gharzouni, I. Sobrados, E. Joussein, S. Baklouti, S. Rossignol, Control of polycondensation reaction generated from different metakaolins and alkaline solutions, J. Ceram. Sci. Technol. 08 (3) (2017) 365–376.
[32] P. Duxson, J.L. Provis, G.C. Lukey, S.W. Mallicoat, W.M. Kriven, J.S.J. van Deventer, Understanding the relationship between geopolymer composition, microstructure and mechanical properties, Colloids Surf. A Aspects 269 (2005) 47–58.
[33] A. Nazari, S. Riahi, A. Bagheri, Designing water resistant lightweight geopolymers produced from waste materials, Mater. Des. 35 (2012) 296–302.
[34] J. Zarzycki, Les verres et l'état vitreux, Masson, Paris, France, 1982.
[35] J. Ye, W. Zhang, D. Shi, Effect of elevated temperature on the properties of geopolymer synthesized from calcined ore-dressing tailing of bauxite and ground-granulated blast furnace slag, Constr. Build. Mater. 69 (2014) 41–48.
[36] T.K. Erdem, Specimen size effect on the residual properties of engineered cementitious composites subjected to high temperatures, Cem. Concr. Compos. 45 (2014) 1–8.